

RSC Advances



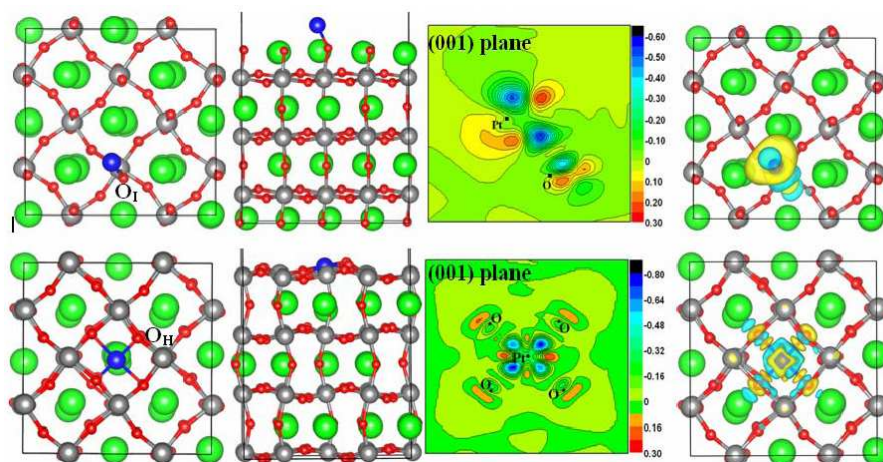
This is an *Accepted Manuscript*, which has been through the Royal Society of Chemistry peer review process and has been accepted for publication.

Accepted Manuscripts are published online shortly after acceptance, before technical editing, formatting and proof reading. Using this free service, authors can make their results available to the community, in citable form, before we publish the edited article. This *Accepted Manuscript* will be replaced by the edited, formatted and paginated article as soon as this is available.

You can find more information about *Accepted Manuscripts* in the [Information for Authors](#).

Please note that technical editing may introduce minor changes to the text and/or graphics, which may alter content. The journal's standard [Terms & Conditions](#) and the [Ethical guidelines](#) still apply. In no event shall the Royal Society of Chemistry be held responsible for any errors or omissions in this *Accepted Manuscript* or any consequences arising from the use of any information it contains.

Graphic abstract



A first-principles study of CO oxidation by surface oxygen on Pt-incorporated perovskite catalyst ($\text{CaPt}_x\text{Ti}_{1-x}\text{O}_3$)

Qiuju Zhang¹, Baihai Li^{1,2}, Houyuan Wang¹, Yange Suo¹, Liang Chen^{1,*}

¹Ningbo Institute of Materials Technology and Engineering, Chinese Academy of Sciences, Ningbo, Zhejiang 315201, P. R. China

²School of Energy Science and Engineering, University of Electronic Science & Technology of China, Chengdu 611731, P. R. of China

Abstract

In the present work, we investigated the structural and catalytic properties of a prototype system Pt-doped CaTiO_3 by means of first principles calculations. We paid particular attention on the aggregation and penetration of Pt on different surfaces of CaTiO_3 , and subsequent CO oxidation by surface oxygen atoms on Pt-doped CaTiO_3 . Our calculations indicate that CO oxidation can potentially take place when Pt is doped on the first layer of $\text{CaTiO}_3(001)$. The activation barriers are calculated to be 0.20~0.45 eV. The possibly induced O vacancy on surface will produce a magnetic behavior by breaking the spin density symmetry due to one Pt-O bond cleavage. Our study is expected to provide an insight of catalytic behavior of Pt ions in Pt-doped perovskite toward the oxidation of exhaust gas.

Keywords: Strong metal-support interaction; Perovskite catalyst; Aggregation; CO oxidation; Pt catalyst

Introduction

Oxide-supported precious-metal particles have attracted intense interest due to their wide applications in heterogeneous catalysis. However, the well-known strong metal-support interactions (SMSI) for group VIII (8-10) noble metals on oxide often drastically reduce their catalytic performance.¹ For example, noble-metal-promoted perovskites, potentially used as automobile exhaust catalysts, exhibit typical SMSI that leads to severe catalyst deactivation.² This deterioration is generally compensated by loading an excess of precious metal, which could result in overconsumption of limited noble metal resources.^{3,4} Therefore, effectively maintaining or increasing the catalytic activity and controlling the consumption of precious metals are highly demanded. Recently, it was observed that the incorporation of precious metal into perovskite lattice is helpful to increase their catalytic ability. The presence of ionic Pd, Pt or Rh in a perovskite matrix, in most cases, is responsible for the high activity of noble-metal-promoted perovskites.^{5,6} For example, BaCeO₃ was experimentally observed to incorporate Pd(II) into B sites to form BaCe_{1-x}Pd_xO_{3-δ}, which maximized the catalytic activity for CO oxidation due to the presence of cationic Pd(II) in the perovskite host.² Similarly, the experimentally observed high-temperature activity of LaPdCoO₃ for lean NO_x reduction was also linked to the presence of ionic Pd in the LaCoO₃ matrix.⁷

Motivated by the high activity of Pd ions in BaCe_{1-x}Pd_xO_{3-δ}, we attempted to investigate the structural and catalytic properties of prototype CaPt_xTi_{1-x}O₃ system by means of first principles calculations. Actually, the incorporation of noble metal into

the B site of perovskite (ABO_3) lattice has been originally found for Pd-doped perovskites ($LaFeCoPdO_3$ and $LaFePdO_3$) due to the self-regeneration abilities of Pd, i.e., Pd could be reversibly incorporated into the perovskite lattice and segregate out, as the exhaust gas is cycled between oxidizing and reducing conditions.^{8,9} The perovskite exhibiting self-regeneration feature is named as “intelligent catalysis” (IC), which was afterward extended to Pt and Rh-doped $CaTiO_3$ systems.⁶ By using x-ray and transmission electron microscope (TEM) techniques, Scott *et al.* observed that Rh or Pt in the doped $CaTiO_3$ could move in and out of the perovskite structure with the fluctuation of oxidation and reduction atmospheres.

In this work, the self-regeneration of single-atom Pt deposition on or penetration into CaO- and TiO_2 -terminated $CaTiO_3$ system was initially studied to evaluate the possibility of the presence of Pt cation. Then the possible enhancement of surface oxygen activity toward CO oxidation by the presence of Pt substitution was explored by performing climbing nudged elastic band (cNEB) method¹⁰⁻¹². The produced oxidation product CO_2 was found to be desorbed from TiO_2 -terminated surface and create an O vacancy, which will induce a spin splitting of Pt-5d electron below the Fermi level, to cause magnetism transformation. Thus, we expect that the magnetism transition from non-magnet of stoichiometric $CaTi_{1-x}Pt_xO_3$ to magnetic $CaTi_{1-x}Pt_xO_{3-\delta}$ can be applied to monitor such oxidation process in the experimental characterization.

II COMPUTATIONAL METHODS

Spin polarized DFT calculations were performed using the Vienna *ab initio* simulation package (VASP).¹³ The electron exchange and correlation were treated

within the generalized gradient approximation (GGA)¹⁴ using the PW91 functional¹⁵⁻¹⁷. The projector-augmented-wave (PAW) method of Blöchl¹⁸ was used for the treatment of the core electrons. A soft potential was employed for oxygen (O_s , $2s^2 2p^4$, cutoff energy of 250 eV), while a plane wave cutoff of 350 eV was chosen in all calculations. Monkhorst Pack (MP) grid¹⁹ of $(2 \times 2 \times 1)$ were used for the (2×2) CaTiO_3 (001) surface. In order to avoid the dipole-dipole interactions between periodic slabs, we built the slab models consisting of 7 atomic layers with CaO or TiO_2 as the termination for both sides. A vacuum spacing of 14 Å was added in the perpendicular direction. All atoms were fully relaxed with the forces converged to less than 0.03 eV/Å. The Methfessel-Paxton technique²⁰ with a smearing width of $\sigma = 0.1$ eV was used to minimize the errors in the Hellmann-Feynman forces. The optimized lattice constants ($a=5.394$ Å, $b=5.512$ Å, $c=7.685$ Å) are in good agreement with experimental results ($a=5.381$ Å, $b=5.442$ Å, $c=7.641$ Å).

To ascertain whether Pt could penetrate into replace CaTiO_3 host to replace Ti ions, the configurations of $\text{CaTi}_{1-x}\text{Pt}_x\text{O}_3$ are generated by the cluster expansion (CE) formalism.²¹⁻²⁴ For the binary system, CE can be written as

$$E(\sigma) = V_0 + \sum_i V_i \sigma_i + \sum_{i,j} V_{ij} \sigma_i \sigma_j + \sum_{i,j,k} V_{ijk} \sigma_i \sigma_j \sigma_k + \dots \quad (1)$$

where V_i , V_{ij} , V_{ijk} , ... are the effective cluster interactions (ECIs), σ is a spin-like occupation variable (e.g., $\sigma = 1$ if the B-site of CaTiO_3 perovskite matrix is occupied by Ti, and $\sigma = -1$ if the site is occupied by Pt). The coefficients are obtained by fitting eqn. (1) to the first principles calculated energies of the selected subset from the configurations generated by CE. In principle, CE should take all the pairs, triplets,

quadruples, etc. into account; however, in practice the cluster expansion can efficiently predict the energy of a system based on fewer coefficients. The optimal coefficient can be obtained according to the cross-validation (CV) score by using a genetic algorithm.^{21,25-28}

III RESULTS AND DISCUSSIONS

A. *Deposition and Migration of Pt on CaTiO₃(001) surfaces*

First of all, we attempt to investigate the binding of Pt atom on the two commonly observed CaO- and TiO₂-terminated surfaces. Similar to the previously studied Pd-doped LaFeO₃ system,^{29,30} the one-fold O_I site at the CaO-terminated surface and the four-fold O_H site at TiO₂-terminated surface are found to be the most favorable binding positions for Pt (see Figure 1). In the calculations, Pt on other trial sites will converge to these two sites upon structural optimizations. As shown in Figures 1 (a) and (b), Pt binds to the outmost O_I on CaO-terminated surface with the bond length of 1.93 Å and tilting angle (\angle PtOO) of about 55°, yielding a binding energy (E_b) of 2.93 eV. In the case of TiO₂-terminated surface, Pt is preferentially located on the O_H hollow site, yielding a slightly higher E_b of 3.10 eV. Upon the deposition of Pt, the four coordinated O_H atoms would be dragged out of surface by around 0.30 Å to form four Pt-O_H bonds with bond lengths in the range of 2.01 ~ 2.05 Å.

Interestingly, the charge distribution analysis displays some distinctive features for the charge transfer between the two surfaces. Specifically, Pt gains 0.55 electron from the CaO-terminated surface, whereas donates 0.63 electron to the TiO₂-terminated surface. This can be understandable since the CaO-terminated and TiO₂-terminated

surfaces are electron-rich and electron-poor, respectively. According to the Bader charge analysis, the net charges on the CaO-terminated and TiO₂-terminated surfaces are calculated to be -0.30 |e| and +0.73 |e|, respectively. In the Bader analysis, each atom is divided based on the zero flux surfaces those are 2-D surfaces on which the charge density is a minimum perpendicular to surface. To present further evidence of electron transfer between Pt and CaTiO₃ surfaces, we also calculated the electron density difference between the adstructures and separate components with each atom frozen at their optimized positions. It is clearly shown in Figures 1(c) and (c') that Pt-O bonds are formed on both surfaces after electron transfer. The 3D yellow spherical shapes (denoting electron-rich area) in Figure 1(d) indicates that Pt serves as electron acceptor on the CaO-terminated surface. In contrast, the light-blue shapes (denoting electron-poor area) of Pt on TiO₂-terminated surface shows electron donating behavior.

Since metal aggregation is usually the major concern for the supported catalysts, we next studied the aggregation tendency of Pt on the two surfaces. As only one favorable binding site is identified for each surface, we evaluated the migration of Pt between two nearest O_I sites on CaO-termination and two nearest O_H sites on TiO₂-termination. The transition state is identified by performing cNEB calculations along the prescribed pathways, as shown in Figure 2. The calculated energy barriers for Pt migration on CaO and TiO₂-terminations are 1.18 and 1.71 eV, respectively. Such high barriers indicate that the migration of Pt is difficult to take place between two nearest O_I or O_H sites. An intermediate state of O-Pt-O bonding is found on the

migration pathway of Pt/TiO₂-term, which is also obtained by the initial optimization as a meta-stable state.

B. The incorporation of Pt into CaTiO₃ lattice

We next estimated the possibility of Pt penetration into the B site of CaTiO₃ lattice in terms of thermodynamics. Here, we calculated the binding energy ($E_b = E_{\text{total}} - E_{\text{vacancy-Ti}} - E_{\text{Pt}}$) for Pt with the Ti vacancy at different layers, as shown in Figure 3(a). E_b is calculated to be 9.52 eV for the substitution of the 1st-layer Ti (denoted as "Pt_{Ti}^{1st}" hereafter), which is increased to 9.81 eV when Pt replaces the second (denoted as "Pt_{Ti}^{2nd}" hereafter) and third layer Ti (denoted as "Pt_{Ti}^{3rd}" hereafter). The larger E_b of Pt_{Ti}^{2nd} and Pt_{Ti}^{3rd} means Pt tend to penetrate deep into the CaTiO₃ lattice, which is consistent with the experimental observation that Pt could dissolve into the CaTiO₃ lattice under oxidizing atmosphere.⁶ Actually, it is reasonable that E_b for Pt_{Ti}^{2nd} is greater than that of Pt_{Ti}^{1st} because Pt forms five Pt-O bonds in a square-pyramid coordination with the bond length of 1.97~2.03 Å in Pt_{Ti}^{1st} while it forms six Pt-O bonds in octahedron coordination with the bond length of 2.02~2.03 Å in Pt_{Ti}^{2nd}.

To further ascertain whether Pt could replace Ti ions of CaTiO₃ and the corresponding stability, we calculated the formation energies of CaTi_{1-x}Pt_xO₃ by DFT methods according to $E_f = E_{\text{CTPO}} - xE_{\text{CPO}} - (1-x)E_{\text{CTO}}$, where E_{CTPO} , E_{CPO} and E_{CTO} are the total energies of CaTi_{1-x}Pt_xO₃, CaPtO₃ and CaTiO₃, respectively, x is the Pt doping concentration. The formation energies obtained by DFT calculations were verified by the CE prediction and a good correlation between them was obtained. The weighted

CV score is 3.3 meV/f.u. with a root mean square (rms) error of 1.4 meV/f.u. in the CE validation process. The comparison between the DFT calculated (red points) and CE predicted (green points) formation energies are shown in Figure 3(b), respectively. The convex hull obtained by CE (green line) is well-converged and accurately reproduces that of the DFT ground states (red line). The negative formation energies of $\text{CaTi}_{1-x}\text{Pt}_x\text{O}_3$ indicate the feasibility of Pt occupying the Ti sites. However, the energy differences between the ground states and other structures are only several meV/f.u., implying that the $\text{CaTi}_{1-x}\text{Pt}_x\text{O}_3$ structures would probably become a disordered solid solution above moderate temperatures.

C. CO oxidation by surface oxygen

Since the lattice oxygen has been verified to not oxidize CO in bare $\text{TiO}_2(110)$ surface³¹, it is natural to ask whether such oxidation process will occur in the presence of ionic Pt in TiO_2 -terminated surface. To explore the possible catalytic enhancement by Pt incorporation into the perovskite host, we focus on the CO oxidation by surface oxygen in $\text{Pt}_{\text{Ti}}^{\text{1st}}$ and $\text{Pt}_{\text{Ti}}^{\text{2nd}}$ TiO_2 -termination. Inspired by the recent observation of single Pt atom loaded on FeO_x nanocrystallite support or graphene to form Pt_1/FeO_x or $\text{Pt}/\text{graphene}$, respectively,^{32,33} we built a model of single Pt atom deposited on the surface or occupying the B site of CaTiO_3 to form $\text{CaPt}_x\text{Ti}_{1-x}\text{O}_3$ to minimize the computational cost and examine its catalytic behavior. We found that CO can be favorably adsorbed on the Pt site to form linear chemisorption state via the C or O ends in the $\text{Pt}_{\text{Ti}}^{\text{1st}}$ structure (see Figure 4(a)). Apparently, the C end can interact with the ionic Pt more strongly, with an adsorption energy ($E_{\text{ads.}} = E_{\text{CTPO}} + E_{\text{CO}} - E_{\text{CO-CTPO}}$) of

1.59 eV and shorter Pt-C distance of 1.86 Å. In contrast, the O end can interact with Pt with an E_{ads} of 0.16 eV and O-Pt distance of 2.13 Å, respectively. For comparison, we also investigated the CO adsorption on Pt deposited onto stoichiometric TiO₂-terminated surface instead of replacing the Ti ion. Upon optimization, the CO molecule initially placed 2.1 Å above the surface Pt atom, would be pushed away in spite of C and O ends, as shown in Figure 4(c), which illustrates that the Pt atom deposited on TiO₂ surface completely loses its reactivity toward CO molecule. Actually, this is reasonable because the four lobes of Pt-5d orbital become inaccessible after the formation of four Pt-O coordination on TiO₂ surface, similar to our previous study of H₂ chemisorption on Pt/MoO₃.³⁴

For the Pt_{Ti}^{2nd} structure, the Pt atom is embraced underneath and not available for interacting with CO. Nevertheless, CO can be still linearly chemisorbed on the Ti site via the C end. The distance between C end and Ti is calculated to be 2.34 Å, as depicted in Figure 4(b). Although the corresponding $E_{\text{ads}} = 0.10$ eV is significantly weaker than that of Pt_{Ti}^{1st}, the reactive activity of Ti is actually enhanced by loading Pt since CO can be hardly adsorbed on the TiO₂-terminated surface of the pure CaTiO₃. The similar phenomenon can be found in the case of CO activation on BaCe_{0.90}Pd_{0.10}O_{3-δ} and undoped BaCeO₃, in which the higher activity associated with BaCe_{0.90}Pd_{0.10}O_{3-δ} is reflected by lower light-off temperature ($T_{50} = 83$ °C), compared with $T_{50} = 225$ °C for the undoped BaCeO₃.²

To ascertain the intrinsic mechanism of the improved surface activity, the 3D electron density difference is plotted for these Pt-doped and undoped structures in

Figure 4. For the $\text{Pt}_{\text{Ti}}^{1\text{st}}$ structure, it is clearly shown that the five-coordinated Pt atom accumulates some electrons (blue contour) along the surface normal (Figure 4(a)) due to the absence of one Pt-O bond. The remained electron on the unsaturated Pt atom is responsible for the high reactivity toward CO adsorption. After further incorporating Pt into the second TiO_2 layer, the surface Ti atom obtains some electrons through the Pt-O-Ti bond (Figure 4(b)), which enhances the reactivity of Ti compared to other surface Ti ions. In contrast, no electron accumulation along the surface normal can be observed nearby the Pt atom deposited on the stoichiometric TiO_2 -terminated surface. As shown in Figure 4(c), only yellow contour of denoting electron deficient in this direction was remained due to the tetra- Pt-O bonds formation.

As discussed above, TiO_2 -terminated surface exhibits electron-poor feature evidenced by Bader charge analysis, which results in the ability of attracting electron in the surface. We next evaluate the possibility of CO oxidation on surface oxygen following the two chemisorption states. For the adstructure (Pt-CO) through C end, the C atom is able to further bind with the neighbored O_1 and drags it out of the surface by about 0.90 \AA to form a bent CO_2 structure, yielding a bent angle $\angle\text{OCO} = 140^\circ$ and E_{ads} of 2.08 eV . We term this state as CO_2 -bending. From the kinetic point of view, the adsorbed CO needs to overcome a barrier of 0.45 eV at the transition state TS_1 to bind with O_1 atom, as depicted in path I of Figure 5. The bond length of two newly formed C-O bonds is slightly elongated from 1.18 \AA to 1.21 \AA due to the slight disturbance of $\text{C}\equiv\text{O}$ triplet bond.

The oxidation process is also found to potentially take place for CO adsorbed

through the O end (Pt-OC). Since adsorption on Pt^{1st} via the O end results in smaller energy, the upstanding C atom will continue to increase its E_{ads} to 0.34 eV by binding with O₁ atom with a bent angle of $\angle\text{OCO} = 106^\circ$. In contrast to the $\eta^2(\text{CO})$ structure, this bent CO₂-TM state should be ascribed to $\eta^2(\text{COO})$ state because the two O atoms are directly bonded with Pt. The newly formed C-O₁ bond of 1.38 Å will also drag the O₁ atom out of TiO₂ surface by about 0.8 Å. The calculated activation barrier of 0.20 eV toward CO oxidation is even smaller than that of the commonly used Au-Cu catalyst (activation barrier = 0.60 eV).³⁵ In the TS_{II}¹, the original C=O bond length is elongated to 1.20 Å and C-O₁ distance is decreased to 2.34 Å. More interestingly, such oxidation state $\eta^2(\text{COO})$ is actually an intermediate and would converge to the most stable CO₂-bending state $\eta^2(\text{CO})$ eventually. The similar conversion has also been found in the previous CO₂-TM state, in which COO binding is not a stable state.^{36,37} In the TS_{II}² (Figure 5), the distance of C-Pt is shortened to 2.67 Å, while the original Pt-O bond is increased to 2.48 Å, yielding an activation barrier of 0.26 eV.

Whether the product (free CO₂ molecule) could be desorbed from such $\eta^2(\text{CO})$ -Pt complex is another key issue for the catalytic activity. As depicted in Figure 5, the CO₂ desorption will increase its thermal energy by about 1.45 eV compared to $\eta^2(\text{CO})$ -Pt complex, yielding an activation barrier of 1.45 eV in this process. Such a high activation barrier is generally difficult to conquer, however, the exothermic energy (about 2.1 eV) of forming $\eta^2(\text{CO})$ in path II possibly accumulate enough energy to enable the desorption of CO₂. It is noteworthy here that the high-barrier reaction pathway II only plays a minor role in the CO oxidation process, compared to

the low-barrier reaction pathway I. Furthermore, an O-vacancy on TiO₂-terminated surface will be induced by CO₂ desorption, as shown in the dashed box in Figure 5. Although no obvious deformation can be discerned except for the slightly elongated bond length of Pt-O bond opposite to Pt-O_{vacancy}, the electron feature near Fermi level is significantly different from the stoichiometric Pt-CaTiO₃. Figure 6(a) clearly shows that the whole electronic bands are downshifted by approximately 0.5 eV in TiO₂-terminated surface with an O-vacancy. An obvious spin splitting at valence band maximum (VBM) is discerned by destroying the symmetric electronic bands of stoichiometric CaTi_{1-x}Pt_xO₃, although the band gap is nearly unchanged. Such electron variation will probably induce magnetism transformation from non-magnet of stoichiometric CaTi_{1-x}Pt_xO₃ to magnetic CaTi_{1-x}Pt_xO_{3-δ}, which is further confirmed by the calculated total magnetic moment of 1.90 μ_B in CaTi_{1-x}Pt_xO_{3-δ}. Projected density of states (PDOS) indicates that the split electronic band in VBM is mainly ascribed to the splitting of Pt-5*d* bands, as shown in figure 6(b), which is consistent with the calculated local magnetic moment of 1.10 μ_B on Pt. Compared to the original smaller peak, Pt-5*d* band becomes more narrow and stronger. Such emergence of magnetism is contributed by the broken symmetric square-pyramid structure of five-coordination of Pt, and is expected to be helpful to monitor the surface oxygen function states in the CO oxidation process.

Conclusion

Based on the DFT and CE calculations, both the increased binding energy with Pt penetration and the negative formation energy of CaTi_{1-x}Pt_xO₃ indicate the feasibility

of replacing Ti sites in CaTiO_3 by Pt, which is consistent with the experimentally observed self-regeneration of Pt particles on CaTiO_3 . The penetrated Pt ion could enhance the surface activity of CaTiO_3 to form two adsorption states through the C and O ends. Further, we show that following oxidation by the surface O atom could readily take place to yield more stable $\eta^2(\text{CO})\text{-Pt}$ complex, due to the low activation barrier of 0.45 eV and 0.20 eV in the pathways I and II. From the whole reaction energy profile, CO oxidation path I is dominate process owing to the lower thermal energy along the oxidation process. However, the minor oxidation path II is possible to induce CO_2 desorption and hence cause a magnetic transition (i.e., from non-magnetic CaTiO_3 to magnetic $\text{CaTiO}_{3-\delta}$). Our study is expected to provide an insight of catalytic behavior of Pt ion in Pt-doped perovskite toward exhaust gas oxidation. The magnetism transition could possibly used as a measurement to monitor the oxidation process.

Acknowledgment

We gratefully acknowledge the financial support by the national key basic research program of China (Grant Nos. 2013CB934800 and 2012CB722700), national science foundation of China (Grant No. 21003144, 11274323), innovative research project of Ningbo municipal government (Grant No. 2011B82005), Ningbo NSF (2012A610117 and 2012A610099), and China postdoctoral science foundation funded project (2013M530292).

Reference

- (1) Tauster, S. J. *Acc. Chem. Res.* **1987**, *20*, 389.
- (2) Singh, U. G.; Li, J.; Bennett, J. W.; Rappe, A. M.; Seshadri, R.; Scott, S. L. *J. Catal.* **2007**,

249, 349.

- (3) Tian, Z. X.; Inagaki, K.; Morikawa, Y. *Curr. Appl. Phys.* **2012**, *12*, S105.
- (4) Li, B.; Ezekoye, O. K.; Zhang, Q.; Chen, L.; Cui, P.; Graham, G.; Pan, X. *Phys. Rev. B* **2010**, *82*, 125422.
- (5) Tanaka, H.; Taniguchi, M.; Kajita, N.; Uenishi, M.; Tan, I.; Sato, N.; Narita, K.; Kimura, M. *Top. Catal.* **2004**, *30-1*, 389.
- (6) Taniguchi, M.; Tanaka, H.; Uenishi, M.; Tan, I.; Nishihata, Y.; Mizuki, J. i.; Suzuki, H.; Narita, K.; Hirai, A.; Kimura, M. *Top. Catal.* **2007**, *42-43*, 367.
- (7) Twagirashema, I.; Engelmann-Pirez, M.; Frere, M.; Burylo, L.; Gengembre, L.; Dujardin, C.; Granger, P. *Catal. Today* **2007**, *119*, 100.
- (8) Nishihata, Y.; Mizuki, J.; Akao, T.; Tanaka, H.; Uenishi, M.; Kimura, M.; Okamoto, T.; Hamada, N. *Nature* **2002**, *418*, 164.
- (9) Tanaka, H.; Taniguchi, M.; Uenishi, M.; Kajita, N.; Tan, I.; Nishihata, Y.; Mizuki, J. i.; Narita, K.; Kimura, M.; Kaneko, K. *Angew. Chem. Int. Ed.* **2006**, *45*, 5998.
- (10) Jonsson, H. *Annu. Rev. Phys. Chem.* **2000**, *51*, 623.
- (11) Henkelman, G.; Uberuaga, B. P.; Jonsson, H. *J. Chem. Phys.* **2000**, *113*, 9901.
- (12) Henkelman, G.; Jonsson, H. *J. Chem. Phys.* **2000**, *113*, 9978.
- (13) Kresse, G.; Hafner, J. *Phys. Rev. B* **1993**, *48*, 13115.
- (14) Perdew, J. P.; Chevary, J. A.; Vosko, S. H.; Jackson, K. A.; Pederson, M. R.; Singh, D. J.; Fiolhais, C. *Phys. Rev. B* **1992**, *46*, 6671.
- (15) Perdew, J. P.; Chevary, J. A.; Vosko, S. H.; Jackson, K. A.; Pederson, M. R.; Singh, D. J.; Fiolhais, C. *Phys. Rev. B* **1993**, *48*, 4978.
- (16) Perdew, J. P.; Burke, K.; Ernzerhof, M. *Phys. Rev. Lett.* **1996**, *77*, 3865.
- (17) Perdew, J. P.; Burke, K.; Ernzerhof, M. *Phys. Rev. Lett.* **1997**, *78*, 1396.
- (18) Blochl, P. E. *Phys. Rev. B* **1994**, *50*, 17953.
- (19) Monkhorst, H. J.; Pack, J. D. *Phys. Rev. B* **1976**, *13*, 5188.
- (20) Methfessel, M.; Paxton, A. T. *Phys. Rev. B* **1989**, *40*, 3616.
- (21) van de Walle, A.; Ceder, G. *J. Phase Equilib.* **2002**, *23*, 348.
- (22) Van der Ven, A.; Thomas, J. C.; Xu, Q. C.; Bhattacharya, J. *Math. Comput. Simul.* **2010**, *80*, 1393.
- (23) Sanchez, J. M.; Ducastelle, F.; Gratias, D. *Physica A* **1984**, *128*, 334.
- (24) Van der Ven, A.; Yu, H. C.; Ceder, G.; Thornton, K. *Prog. Mater. Sci.* **2010**, *55*, 61.
- (25) Hart, G. L. W.; Blum, V.; Walorski, M. J.; Zunger, A. *Nature Mater.* **2005**, *4*, 391.
- (26) Xu, Q.; Van der Ven, A. *Phys. Rev. B* **2007**, *76*, 064207.
- (27) Van der Ven, A.; Thomas, J. C.; Xu, Q. C.; Bhattacharya, J. *Math. Comput. Simul.* **2010**, *80*, 1393.
- (28) Sanchez, J. M.; Ducastelle, F.; Gratias, D. *Physica A* **1984**, *128*, 334.
- (29) Van der Ven, A.; Yu H. C.; Ceder, G.; Thornton, K. *Prog. Mater. Sci.* **2010**, *55*, 61.
- (30) Li, B.; Katz, M. B.; Zhang, Q.; Chen, L.; Graham, G. W.; Pan, X. *J. Chem. Phys.* **2013**, *138*, 144705.
- (31) Wu, X. Y.; Selloni, A.; Nayak, S. K. *J. Chem. Phys.* **2004**, *120*, 4512.
- (32) Qiao, B.; Wang, A.; Yang, X.; Allard, L. F.; Jiang, Z.; Cui, Y.; Liu, J.; Li, J.; Zhang, T. *Nature Chem.* **2011**, *3*, 634.
- (33) Sun, S.; Zhang, G.; Gauquelin, N.; Chen, N.; Zhou, J.; Yang, S.; Chen, W.; Meng, X.; Geng,

D.; Banis, M. N.; Li, R.; Ye, S.; Knights, S.; Botton, G. A.; Sham, T.-K.; Sun, X. *Sci. Rep.* **2013**, *3*.

(34) Li, B.; Yim, W.-L.; Zhang, Q.; Chen, L. *J. Phys. Chem. C* **2010**, *114*, 3052.

(35) Hussain, A. *J. Phys. Chem. C* **2013**, *117*, 5084.

(36) Zhang, Q.; Cao, L.; Li, B.; Chen, L. *Chem. Sci.* **2012**, *3*, 2708.

(37) Gibson, D. H. *Chem. Rev.* **1996**, *96*, 2063.

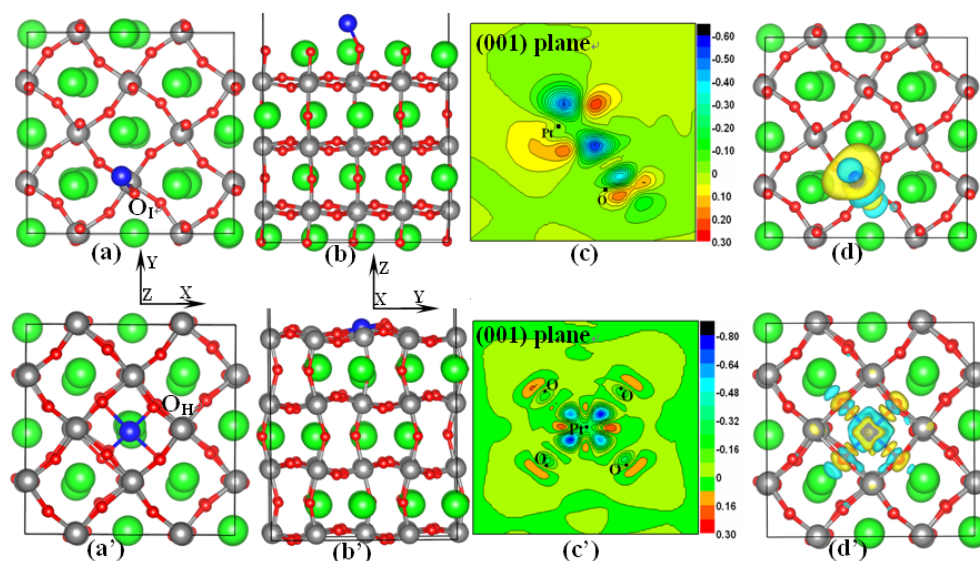


Figure 1 Single Pt atom adsorption on CaO and TiO₂-terminated surface. (a)~(d) provide the topview and sideview of single Pt atom deposition on CaO-terminated surface, and its 2D and 3D electron energy difference; (a')~(d') shows the corresponding parts of single Pt atom deposition on TiO₂-terminated surface. The green, grey, red and blue balls represent Ca, Ti, O and Pt atoms, respectively.

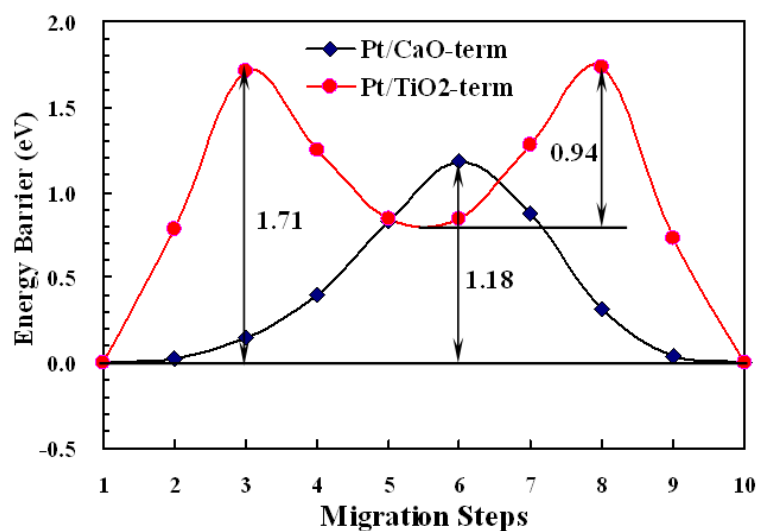


Figure 2 The migration barriers of single Pt atom between the nearest O_I and O_H sites on CaO- and TiO₂-terminated surface, respectively.

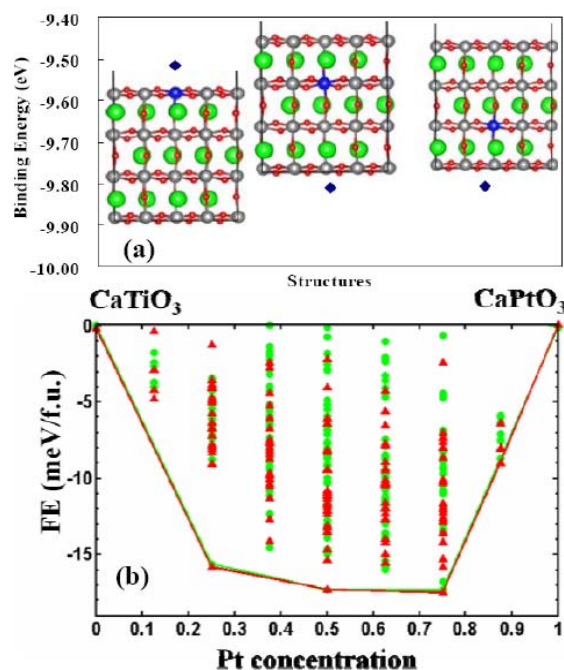


Figure 3 (a) The structures of Pt penetration into different layer Ti to form Pt-CaTiO₃; (b) Convex hulls of the formation energies per formula unit (FE/f.u.) of Pt doped CaTiO₃ structures based on first principles calculation and cluster expansion. Data obtained by VASP and CE are colored red and green, respectively.

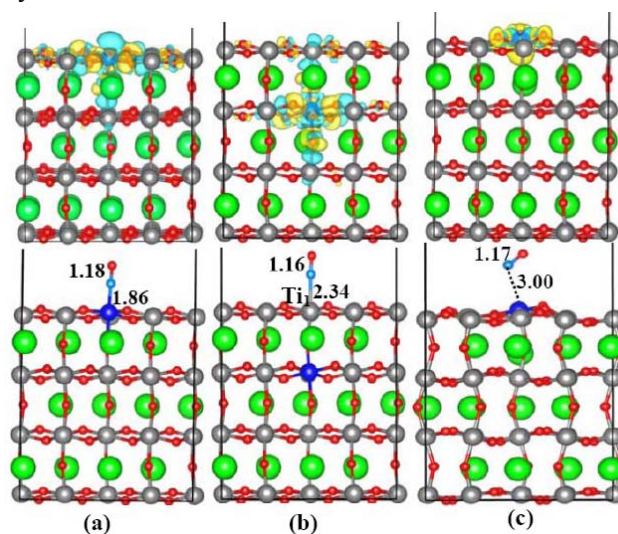


Figure 4 The bottom presents adstructures of CO adsorption on Pt_{Ti}^{1st}, Pt_{Ti}^{2nd} and Pt deposition on TiO₂-terminated surface through C end. The top is the corresponding calculated 3D electron density difference of Pt-doped CaTiO₃(001) with TiO₂-termination.

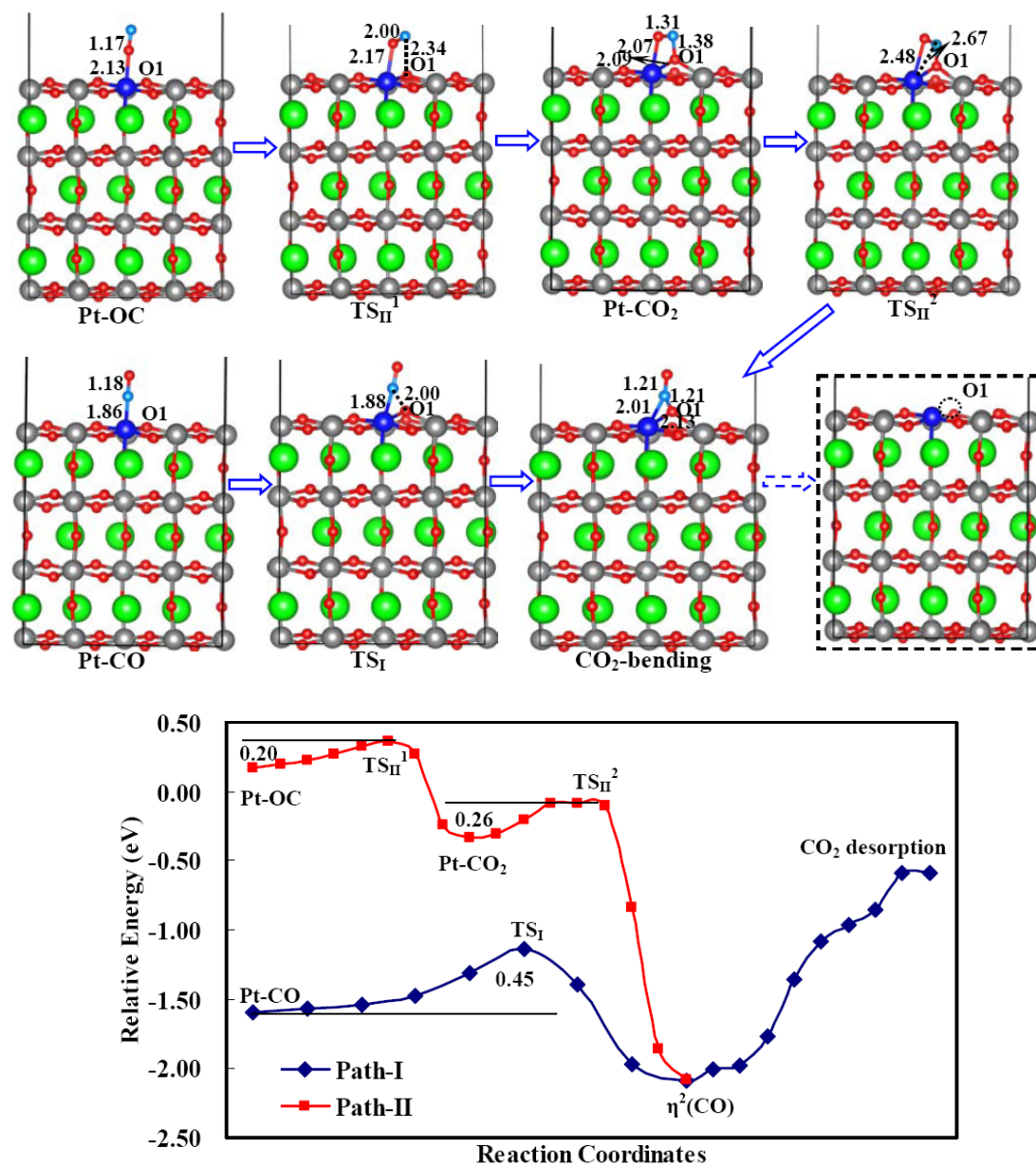


Figure 5 The CO oxidizing process by the surface O1 atom on TiO₂-terminated surface of Pt-substitution the first layer Ti. Path I and II refer to the two reaction pathways through C and O ends. The corresponding structures and the bond length are also presented.

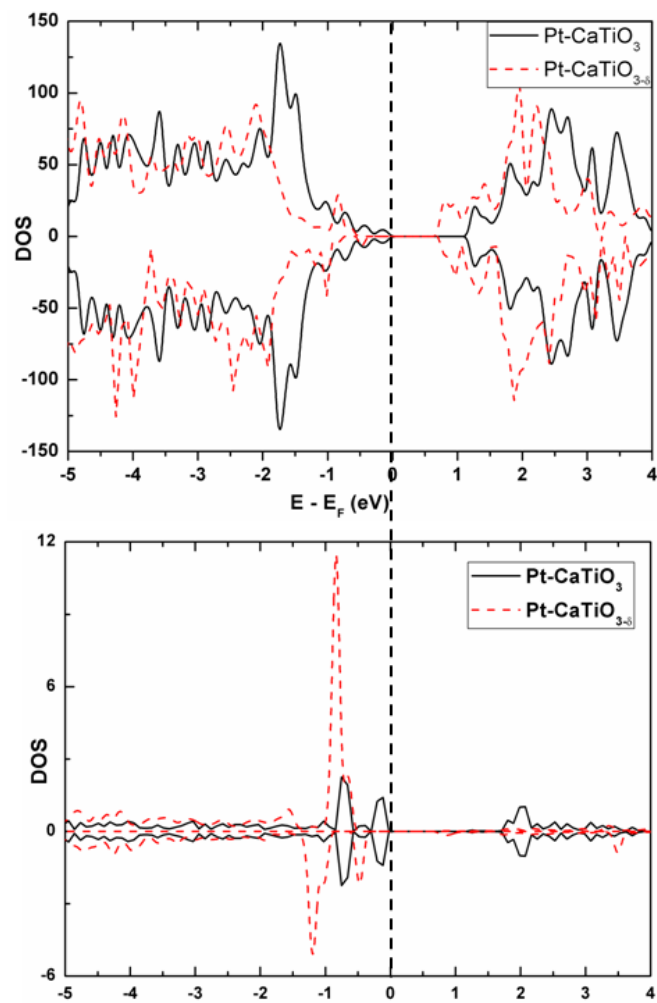


Figure 6 The total density of states (TDOS) for O-vacant (Pt-CaTiO_{3-x}) and projected local density of states (PDOS) comparison of Pt-5d band to illustrate their electromagnetic behavior near Fermi level.